Cite this article
Fan S, Bienen B and Randolph MF
Centrifuge study on effect of installation method on lateral response of monopiles in sand.
International Journal of Physical Modelling in Geotechnics,
https://doi.org/10.1680/jphmg.19.00013

Research Article
Paper 1900013
Received 22/03/2019;
Accepted 19/08/2019

Keywords: foundations/offshore engineering/piles & piling

International Journal of Physical Modelling in Geotechnics

ice Publishing

Centrifuge study on effect of installation method on lateral response of monopiles in sand

Shengsheng Fan BEng, MSc
PhD candidate, Centre for Offshore Foundation Systems, Oceans Graduate School, The University of Western Australia, Crawley, Perth, WA, Australia (corresponding author: shengsheng.fan@research.uwa.edu.au) (Orcid:0000-0002-6316-2790)

Britta Bienen BEng, Dipl.-Ing, PhD
Associate Professor, Centre for Offshore Foundation Systems, Oceans Graduate School, The University of Western Australia, Crawley, Perth, WA, Australia (Orcid:0000-0002-0342-0698)

Mark F. Randolph MA, PhD, FAA, FREng, FRS, FTSE, FIEAust, CPEng
Professor, Centre for Offshore Foundation Systems, Oceans Graduate School, The University of Western Australia, Crawley, Perth, WA, Australia (Orcid:0000-0003-3136-6454)

Monopiles used as foundations for offshore wind turbines can be installed using different methods including jacking, vibratory driving and impact driving. Significant research efforts have been dedicated to the characterisation of monopile–soil interaction under lateral loading, mainly using *p–y* curves. There has also been extensive research in quantifying the effect of different installation methods on the axial response using numerical modelling and physical modelling techniques. Little attention has been paid to the effect of the installation method on the subsequent lateral response of a monopile under the in-service condition. In this paper, a purpose-designed apparatus is described that allows in-flight installation using different installation methods followed directly by lateral loading without stopping the centrifuge and thus retaining the installation-induced stress state. Test results from three lateral loading tests are discussed, with the piles either jacked at 1*g* and *Ng* or impact driven at *Ng* into a dry medium dense sand, allowing the effect of the installation method on the initial stiffness and ultimate capacity to be examined. The successfully conducted tests illustrate the capabilities of the new apparatus for centrifuge testing of laterally loaded driven piles.

Notation

A	pile total (gross) cross-sectional area, $\pi D_{\text{pile}}^2/4$ (m^2)
D	pile outer diameter (steel) (m)
D_{pile}	overall pile diameter (including epoxy) (m)
D_{R}	relative density of sand (dimensionless)
d_{50}	mean grain/particle size (mm)
EI	bending stiffness (N m^2)
e	load eccentricity (m)
$\boldsymbol{F}$	penetration resistance or driving force (N)
G	shear modulus (GPa)
$\boldsymbol{g}$	gravitational acceleration
H	lateral load (N)
k_{ini}	initial stiffness (dimensionless)
k_{ult}	secant stiffness (dimensionless)
L	pile embedment length (m)
M	bending moment (N m)
N	$\boldsymbol{g}$ level (dimensionless)
$\text{RP}_{0\cdot2}$	proof stress at 0·2% plastic strain (MPa)
$\text{RP}_{1\cdot0}$	proof stress at 1·0% plastic strain (MPa)
T	overall pile wall thickness (including epoxy) (m)
t	pile wall thickness (m)
t_1	epoxy coating thickness (m)
U	index of uniformity (dimensionless)
z	distance above mudline (m)
z_1	distance above mudline (laser 1) (m)
z_2	distance above mudline (laser 2) (m)
δ	pile deflection (m)
γ	sample dry density (kN/m^3)
$\gamma_{\text{d max}}$	maximum dry density (kN/m^3)
$\gamma_{\text{d min}}$	minimum dry density (kN/m^3)
κ	Timoshenko shear coefficient (dimensionless)

1. Introduction

The offshore wind energy market has been expanding rapidly due to the need for sustainable and cleaner energy sources globally. In 2017, twice as much additional net capacity as 2016 was installed, comprising 560 offshore wind turbines across 17 wind farms (EWEA, 2017). Monopiles remain the most prevalent foundation type for offshore wind turbines, accounting for 87% of all installations.

Significant research efforts have been dedicated to the characterisation of monopile–soil interaction under lateral loading, mainly using *p–y* (load–displacement) curves. These were originally developed for long, slender, small-diameter piles undergoing a limited number of load cycles (API, 2011;

Matlock, 1970; Reese *et al.*, 1974). In contrast, large-diameter monopiles for offshore wind turbines are of relatively low embedment (typically less than 5 diameters) and operational loading involves a high moment-to-load ratio, with eccentricity of several diameters. Monopiles therefore tend to behave more rigidly, and with a dominant component of rotation, so that the p–y curves developed from near-surface loading of slender piles are of questionable applicability (Achmus *et al.*, 2009; Achmus and Abdel-Rahman, 2005; Byrne *et al.*, 2015; LeBlanc *et al.*, 2010; Zdravković *et al.*, 2015, among others). Moreover, monopiles are subjected to millions of load cycles over the 25-year design life, requiring the accumulated rotation and stiffness change under a long-term cyclic loading to be predicted. Furthermore, the effect of pile installation on the subsequent response of monopiles under lateral loading is not accounted for, although design guidelines such as DNV (2014) acknowledge that the method of installation should be considered in the design of pile foundations. Recently, a modified p–y method has been developed as an outcome of the PISA (pile–soil analysis) joint industry project (Byrne *et al.*, 2017). That study targeted monopiles and included onshore testing of driven piles subjected to monotonic push-over loading in sand and clay (with a maximum pile diameter $D = 2$ m and embedded lengths $L \leq 5{\cdot}25$D). However, pile installation effects were ignored in the numerical simulations that formed the basis of new prediction methods, which were performed as wished-in-place small strain analyses.

Research on the lateral response of monopiles has made widespread use of model tests. In the majority of published tests, the monopiles were installed by jacking at 1$\boldsymbol{g}$, although it is known that the state of the surrounding soil is significantly influenced by the pile installation method (Henke and Bienen, 2013; Labenski *et al.*, 2016). As a result, the subsequent lateral response of monopile may be affected. Little has been published on the effect of the installation process on the subsequent lateral response of piles, although it is well known that the axial response is strongly influenced by the installation method (De Nicola and Randolph, 1997; Henke and Bienen, 2013; Henke and Grabe, 2008; Mahutka *et al.*, 2006). Where piles were jacked or impact-driven in-flight in centrifuge tests (Dyson and Randolph, 2001; Klinkvort, 2012), the tests required stopping of the centrifuge to mount the lateral loading rig. Hence, the soil state following pile installation was likely changed due to the stress-level changes in the soil sample. Further disturbance may have occurred when mounting the testing equipment. Hence, the effect of the pile-installation process on the lateral response still holds significant uncertainty.

To address this issue, an experimental apparatus is needed that allows both in-flight installation and lateral loading of monopiles without stopping the centrifuge. This paper introduces such a purpose-designed apparatus for centrifuge model tests and examines the effect of pile installation on the subsequent lateral response of monopiles. The test results allow the quantification of the effect of pile installation on the initial stiffness and ultimate capacity of monopiles under lateral loading and highlight the potential for using centrifuge modelling techniques for this problem.

In the following, all dimensions and displacements are presented at equivalent prototype scale unless otherwise noted.

2. Development of experimental loading apparatus

The experiments can be divided into two phases, namely an installation phase and a horizontal loading (in-service) phase. A purposed-designed apparatus which can meet the test requirements has been developed, as described in the following.

2.1 Development of the pile-driving hammer

2.1.1 Existing miniature centrifuge pile-driving hammer

Pile installation in the centrifuge including impact driving and jacking has been achieved using a purpose-built miniature pile-driving hammer that is mounted on a centrifuge actuator (Bruno and Randolph, 1999; De Nicola and Randolph, 1994). This apparatus was also used by Henke and Bienen (2013) and Heins *et al.* (2018). However, it was designed originally for axial loading following pile installation, without considering lateral loading. Therefore, it needed to be modified for this study due to the following constraints: first, the pile head and driving hammer (anvil) were rigidly connected. This resulted in a fixed-end (zero relative rotation) boundary condition which is not representative of monopiles in the field. Second, very limited lateral load could be applied through the pile-driving hammer, which would be insufficient for push-over testing of monopiles.

2.1.2 Requirements for the modified pile-driving hammer

To overcome the constraints mentioned above, modifications of the existing pile-driving hammer were required. The modified pile-driving hammer should be capable of modelling the entire pile installation process and freeing up the pile head for the lateral loading stage in-flight after installation. The modified pile-driving hammer therefore needs to be able to

(*a*) suspend the pile above the soil surface during ramping up and before installation, allowing installation to start from the soil surface
(*b*) allow for pile penetration into the soil under its self-weight
(*c*) apply the installation force, through jacking or impact driving

(*d*) release the connection between the pile head and the pile-driving hammer in-flight, allowing the pile to sit freely under its self-weight.

2.1.3 Modifications of the pile-driving hammer

The pile-driving hammer developed by De Nicola and Randolph (1994) was modified so that the pile head could be freed after installation. Instead of a rigid threaded connection, a flexible connection that could be released was used in the experiments described here. Figure 1(a) shows the rigid connection between the pile tip and the anvil. The modified connection that frees the pile head following installation is shown in Figure 1(b). The anvil is extended by a steel claw (item 3) and a connector (item 4) is added to the pile head. The monopile hangs on the claw of the connector before initiating installation, allowing the pile to be suspended above the soil surface during centrifuge spin-up. Installation is effected through the compression connection once the connector is in contact with the inside top of the claw. After installation, the steel claw is lifted up in-flight through the vertical movement of the actuator until the pile connector sits centrally in the space within the claw. As a result, clearance of around 8 mm is created at both the top and bottom of the connector head, which is sufficient to release any constraint on the pile head. Details of the connection are shown in Figure 1(c).

2.2 Development of the lateral loading rig

2.2.1 Requirements for the new lateral loading rig

Monopile lateral loading tests have been conducted using different experimental arrangements (Bienen *et al.*, 2012; Dyson and Randolph, 2001; Klinkvort, 2012). However, these tests required stopping of the centrifuge to mount the lateral loading rig. As a result, the soil state was likely changed. To maintain the stress states induced by pile installation, lateral loading should be applied without stopping the centrifuge.

Monopiles for offshore wind turbines are subjected to complex wind, wave and current loads from the ocean environment. This requires a facility for cyclic load application, although monotonic lateral load was considered for this first series of tests to obtain the full load–displacement curve to ultimate capacity, allowing changes in stiffness to be evaluated as well.

In the absence of a multi-tool in-flight robot (Gaudicheau *et al.*, 2013), to allow lateral loading to be carried out directly following installation, the loading device needs to

(*a*) be mounted on the actuator from the start – that is, in-place before pile driving
(*b*) not disturb the pile installation process and
(*c*) allow both monotonic and cyclic loading.

2.2.2 Details of the lateral loading rig

A loading yoke similar to that used by Dyson and Randolph (2001) and Bienen *et al.* (2012) was manufactured to meet the aforementioned requirements, as shown in Figure 2. In the previous studies, the loading yoke was mounted on the actuator carriage. This was not possible here, as the vertical degree of freedom of the actuator was used solely for pile installation and any use during the lateral loading phase would have conflicted with the pile movement. The loading rig, consisting of a

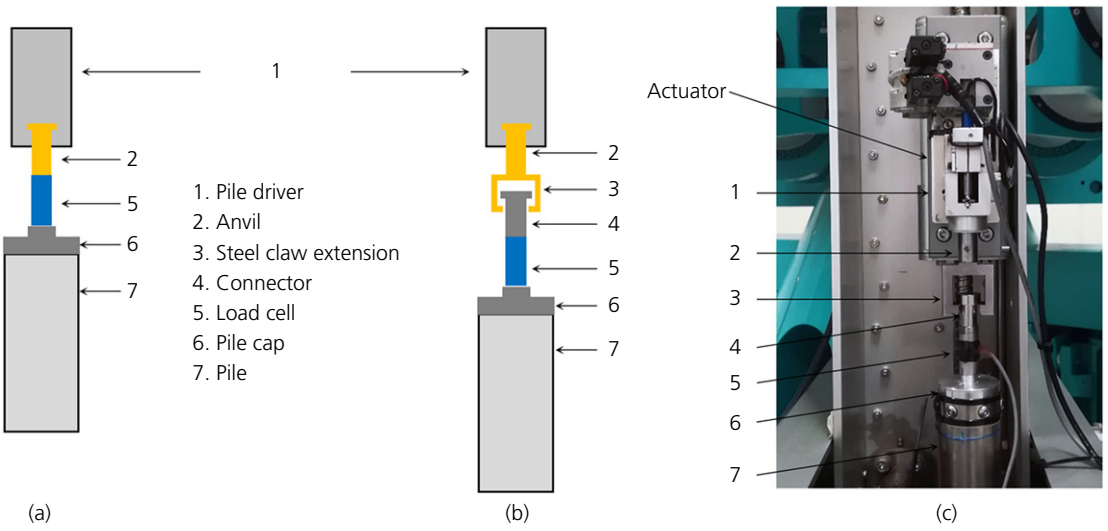

Figure 1. Connection between the pile driver and the pile: (a) rigid connection, (b) modified connection used in this study and (c) photograph of connection details

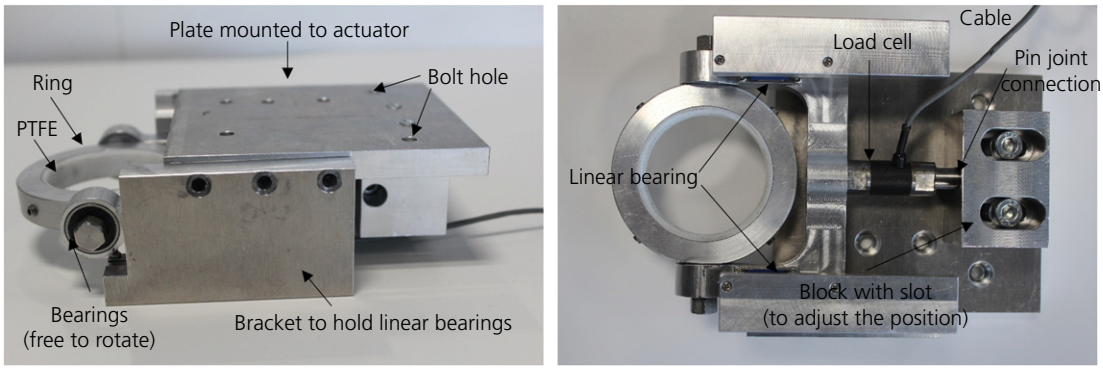

Figure 2. Details of the lateral loading rig: (a) side view and (b) view from below. PTFE, polytetrafluoroethylene

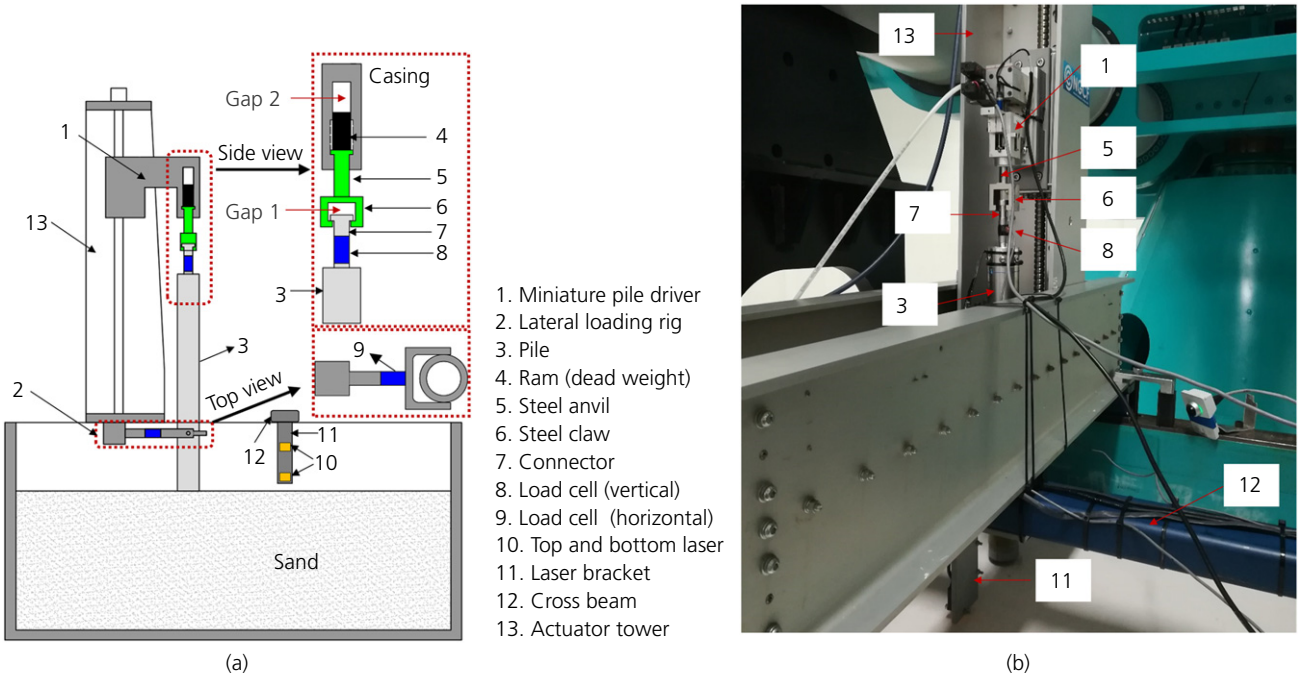

Figure 3. Experimental arrangement: (a) schematic and (b) photograph

free head loading yoke and a connection piece (Figure 2), was therefore mounted on the bottom plate of the actuator as shown in Figure 3.

This configuration increases significantly the magnitude of the lateral load that can be applied as all the loads are taken by the horizontal lead screw rather than being transferred through the pile-driving hammer. More importantly, the loading rig can be mounted in-place initially without influencing the pile installation, and also acts as an installation guide. The internal diameter of the loading yoke is slightly larger than the pile diameter to accommodate slight imperfections in the pile outer diameter or roundness. The size of the pile necessitates a relatively large and thus heavy loading yoke. Therefore, a pair of miniature linear bearings (as shown in Figure 2(b)) was attached to the bottom plate of the actuator to support the connection piece, thus eliminating any effect of the yoke self-weight on the accuracy of the lateral force measurement. The loading yoke can move freely on the linear guides. The general arrangement of the complete apparatus is shown in Figure 3.

2.3 Instrumentation of the experimental apparatus

2.3.1 Load measurements

The driving force was measured using a 10 kN load cell connected to the pile cap (see Figures 1 and 3). The jacking force was obtained directly from the load cell reading recorded by the data-acquisition system (DIGDAQ). A high-frequency sampling rate is required to capture the transient peak driving force during impact driving (Bruno and Randolph, 1999). This is only achievable for a limited number of blows as the data file becomes extremely large and the logging system can become unstable. Therefore, the transient peak impact force was measured in a calibration test conducted to check the hammer-driving efficiency (see Section 4) but not during the centrifuge tests.

The lateral load was measured using a 3 kN load cell connected to the loading yoke (see Figures 2 and 3).

2.3.2 Displacement measurements

During the installation phase, the pile displacement can be derived from the vertical actuator motor encoder. This allows the embedment length to be calculated. During the lateral loading phase, the lateral displacements at two elevations were measured with two laser displacement sensors (KEYENCE LB-11). Determination of pile head displacement and rotation from these measurements is discussed in Section 4.

2.4 Limitations of the loading apparatus

The apparatus meets the requirements stated earlier in this paper. However, some limitations still remain.

(*a*) The maximum achievable jacking force is around 7·0 kN, which is constrained by the integrity of the actuator and the pile-driving hammer.
(*b*) The maximum achievable impact-driving force is currently around 25 MN (2·5 kN in the model scale). This is constrained by the size of the hammer, including the drop height and ram weight.
(*c*) The maximum pile-driving frequency is limited to 15 Hz (in the model scale).

Modification of these specifications would require a new miniature pile-driving hammer to be designed and built. As a consequence, jacked and driven installation into dense sand may result in limited embedment depth due to the high penetration resistance.

3. Model test

3.1 Facility

Experiments were conducted in the 10 m dia. beam geotechnical centrifuge (C72 Centrifuge) at the National Geotechnical Centrifuge Facility (NGCF), hosted by the Centre for Offshore Foundation Systems at the University of Western Australia (Randolph and Gaudin, 2017). An acceleration of 100$\boldsymbol{g}$ was defined at 2/3 of the initial target embedment length (250 mm) from the soil surface.

3.2 Test arrangement

All tests were conducted in a strongbox with internal dimensions of 1000 mm × 1000 mm in plan and 478 mm deep. A side view of the lateral loading test layout (post installation) is shown in Figure 4. The pile is shown schematically, with details given later. The embedment length (L) and the load eccentricity (e) were maintained the same for all tests, allowing the test results to be compared directly. The displacement sensors were mounted on a bracket attached to a cross beam (items 11, 12 in Figure 3).

3.3 Model monopile and instrumentation

Details of the model monopile are shown in Figure 5. The steel monopile has an outer diameter (D) of 50 mm and a wall thickness (t_0) of 1·0 mm. The corresponding diameter-to-wall thickness ratio (D/t) is 50. This represents a prototype monopile with a diameter of 5·0 m and a wall thickness of 0·1 m when tested at 100$\boldsymbol{g}$. The total length of the pile is 500 mm (10D). The dimensions of the model monopile are similar to monopiles used in field conditions (Byrne *et al.*, 2015), although the D/t ratio of the steel itself is slightly higher. The model pile is made from a welded pipe using V2A-steel (material number 1·4301). It has a proof stress of around 200 MPa ($RP_{0·2} = 190$ MPa; $RP_{1·0} = 225$ MPa), according to European standard DIN EN 10088-3 (DIN, 2014). Young's modulus is around 200 GPa. Standard high-strength steel tubes or alloy pipes available with the specified diameter tend to have a larger wall thickness. These were deemed unsuitable for this study as a pile with larger wall thickness would lead to a higher penetration resistance, and not reflect typical pile–soil stiffness ratios under lateral loading.

Ten pairs of full bridge strain gauges (Dual Parallel Grids Strain Gage, SGT-3/350-DY41) were attached to the pile external surface to measure the bending moment, with gauge locations shown in Figure 5. The gauges and wires are protected by a 1·1 mm (t_1) thick layer of epoxy coating as the full testing programme includes experiments in saturated sand. The epoxy coating leads to an increase in the wall thickness. As a result, the overall pile diameter ($D_{pile} = D + 2t_1$) and wall thickness ($T = t_0 + t_1$) are 52·2 and 2·1 mm, respectively. This actually has a beneficial effect of increasing the effective D/t ratio to 60, which is more typical of monopiles near the seabed surface; note that Young's modulus of the epoxy is much lower than for steel so that it has a negligible effect on the pile-bending stiffness.

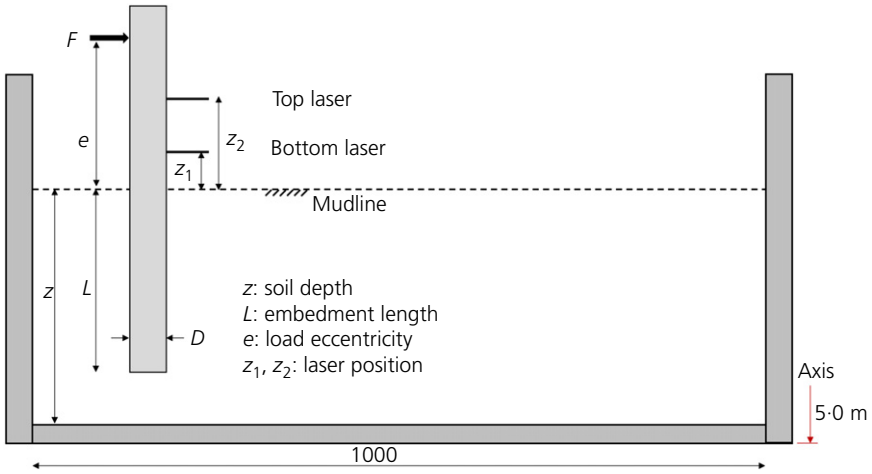

Figure 4. Side view of test layout (post-installation)

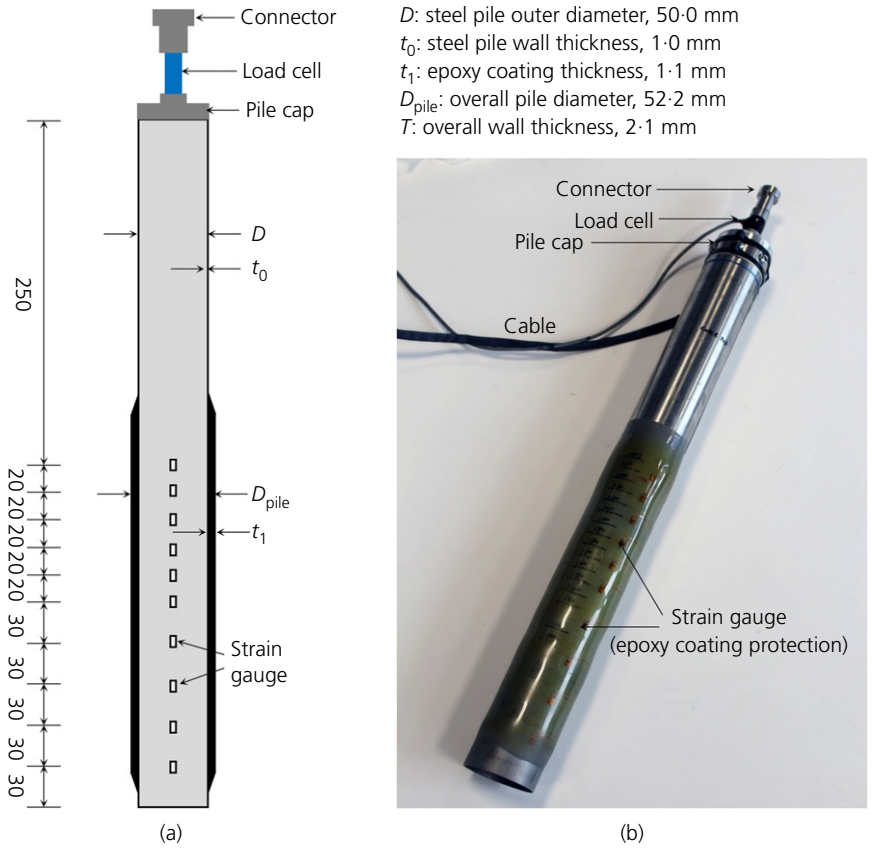

Figure 5. Details of the model monopile

The roughness of the external epoxy surface and the internal pile steel surface (mill finished) was 0·80 and 0·31 μm, respectively. The normalised surface roughness is in the range 0·0016–0·0042. The pile is smoother than a standard offshore pile, for which the normalised surface roughness lies typically in the range 0·02–0·03 (De Nicola and Randolph, 1997).

Table 1. Properties of very fine UWA silica sand

Parameter	Value	Description
d_{50}	0·18	Mean particle size: mm
U	1·67	Index of uniformity
$\gamma_{d\ min}$	14·7	Minimum dry density: kN/m^3
$\gamma_{d\ max}$	17·4	Maximum dry density: kN/m^3

Source: Chow *et al.* (2018)

3.4 Soil preparation and characterisation

All tests were conducted in dry, very fine UWA (University of Western Australia) silica sand with properties summarised in Table 1. The pile diameter-to-mean grain-size ratio D/d_{50} is 278. The effect of the particle size can be neglected if D/d_{50} is larger than 60–100 (Dyson and Randolph, 2001; Verdure *et al.*, 2003). A 'modelling of model' study conducted by Klinkvort and Hededal (2010) suggests a ratio of the pile diameter and mean particles greater than 105 is sufficient to minimise the scale effect for short stiff piles. Ideally, the ratio of wall thickness to mean particle size t/d_{50} should be larger than 10 (De Nicola, 1996; De Nicola and Randolph, 1997) to avoid particle-size effect on the interaction between the pile annulus and the soil. However, the wall thickness of the model pile is only 1% prototype size, which makes it impractical to meet the given criterion exactly. Therefore, a balance was struck between maintaining geometry similitude and avoiding potential particle-size effect, resulting in a ratio of pile annulus to mean particle size of 5·6. Tran (2005) showed that variations in the absolute wall thickness of a suction caisson did not affect the installation response significantly. Thus, the effect of the wall thickness on the pile installation is judged to be minor in this study.

A medium dense sand sample was used to minimise the penetration resistance in the tests discussed in this paper. The sample was prepared loose by pouring the sand into the strongbox carefully by hand with a scoop at the minimum dropping height. Following transferral to the centrifuge basket, the sample was spun up and down several times to limit further densification over the course of the testing programme.

The sample was calibrated by in-flight cone penetration tests (CPTs) using a 7 mm dia. miniature cone penetrometer. The cone (tip) resistance profiles are shown in Figure 6. The relative density was evaluated according to the correlation of the relative density with cone resistance after Schneider and Lehane (2006). The estimated relative density is $D_R = 38 \pm 4\%$.

3.5 Test programme and procedure

3.5.1 Pile installation

The monopile was installed in-flight through jacking or impact driving using the modified pile-driving hammer. A test

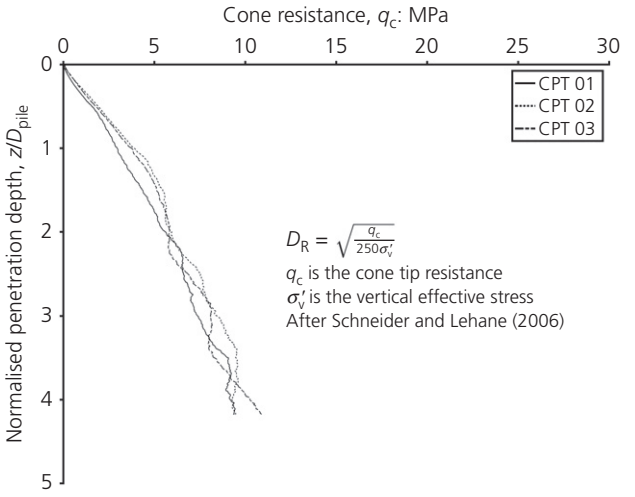

Figure 6. CPT profiles

featuring jacked installation at 1***g*** was conducted for comparison. The jacked installation was performed by applying a constant penetration rate of 0·5 mm/s through the pile-driving hammer and actuator. A ram weight of 0·05 kg and drop height of 17 mm, in model scale, was used for the impact driving test. This corresponds to a ram weight of 50 t and drop height of 1·7 m in prototype scale when tested at 100***g***. The driving frequency was 5 Hz (model scale).

The maximum penetration resistance was expected for the jacked installation at $N\boldsymbol{g}$. The jacked installation was stopped when the penetration resistance approached the actuator capacity. A penetration of 15·9 m ($L \approx 3{\cdot}1D_{pile}$) was achieved. The embedment length in the 1***g*** jacked installation and $N\boldsymbol{g}$ impact driving tests was maintained the same to enable the direct comparison of the response under lateral loading.

3.5.2 Pile lateral loading

After installation, the pile head was released as described earlier and the quasi-static monotonic lateral loading was applied using the loading yoke until the monopile mudline displacement exceeded $0{\cdot}1D_{pile}$. The lateral load (H) was applied at an eccentricity $e = 3{\cdot}8D_{pile}$ above the soil surface. The resulting bending moment at mudline is $M = He$.

3.5.3 Test procedure details

The experiments were performed according to the following procedure.

- The pile was supported on the steel claw while the centrifuge ramped up to the target acceleration level. The pile was suspended just above the soil surface until installation was initiated.

- The pile penetrated into the soil under its self-weight. This was achieved by requesting the vertical actuator to travel downwards slowly (at a rate of 0·1 mm/s).
- The procedures for jacked installation and impact driving are slightly different.
  (*a*) Jacked installation: as the assembly continued to move, the additional weight of the steel claw (anvil) and the ram were transferred gradually to the pile, resulting in further penetration. Once the ram had lifted to reach the inside top of the casing (gap 2 closed, Figure 3(a)), the compression connection was established and the constant displacement rate of the actuator was transferred to the pile. Pile jacking was terminated as the driving resistance approached the actuator capacity.
  (*b*) Impact driving: the pile-driving hammer continued to move until the anvil was elevated by a distance (clearance) of around 3 mm. The pile-driving hammer was activated and impact driving started. The control system allows the vertical actuator to follow the penetrating pile, maintaining the specified impact drop height, using the displacement transducer within the pile-driving hammer. The driving process was stopped when the same penetration depth as the ***Ng*** jacked installation was achieved.
- After installation, the steel claw was lifted up by the pile-driving hammer by moving the vertical actuator upwards. This created the required clearance around the pile head connector for the lateral loading phase.
- The lateral loading was then applied through the loading yoke. This was achieved by moving the horizontal actuator at a controlled rate of 0·01 mm/s. This is sufficiently slow to ensure a quasi-static pile response.

All operations including the pile installation and the lateral loading were performed without stopping the centrifuge. For comparison, a test featuring jacked installation at 1***g*** was included (using the same procedure as in the ***Ng*** jacked installation but ramping the centrifuge up only for the lateral loading phase, the main difference being the stress level during installation). A summary of tests conducted is given in Table 2.

Table 2. Details of tests conducted

Test number	Installation phase	Lateral load phase
1	Jacking at 100***g***	Monotonic push over at 100***g***
2	Jacking at 1***g***	Monotonic push over at 100***g***
3	Impact driving at 100***g***	Monotonic push over at 100***g***

Notes: 1, sample relative density: 38 ± 4% after Schneider and Lehane (2006), average unit weight $\gamma = 15{\cdot}0$ kN/m^3; 2, achieved embedment length was $3{\cdot}1D_{pile}$ in test 1, which was kept the same for tests 2 and 3; 3, load eccentricity is $3{\cdot}8D_{pile}$

4. Experimental results and discussions

4.1 Pile installation history

4.1.1 Jacked installation

Figure 7 presents the penetration resistance reported during 1***g*** and ***Ng*** jacked installation. The penetration depth is normalised by the overall pile diameter (D_{pile}). The jacking force and impact driving force discussed in the following are normalised as stress by dividing the force by the gross cross-sectional area (A). The penetration resistance reported is the sum of the tip resistance and the shaft resistance. A penetration of 15·9 m in prototype scale (159 mm in model scale, $L = 3{\cdot}1D_{pile}$) was achieved. A significant difference is observed when comparing the results of piles jacked at 1***g*** and ***Ng***, with the jacking force required for in-flight installation around 40 times higher than that in the 1***g*** jacked installation. Similar results were reported by Haffar *et al.* (2017), where the effect of the stress level on the response of pile installation was investigated. The axial capacity of the piles was estimated using the UWA-05 method (Lehane *et al.*, 2005), resulting in a value (normalised by A) of around 2·2 MPa. However, this should be considered a lower bound on the expected capacity, since the method is aimed at driven piles, where the cyclic nature of the installation process will give much greater friction degradation than for a jacked pile. Indeed, the measured bearing capacity is 3·1 MPa, which is 43·9% higher.

Although no direct observation of the internal soil plug was possible in the experimental set-up, the penetration resistance may be used to gauge the degree of plugging during jacking. Assuming a shaft friction ratio of 1% of the cone resistance,

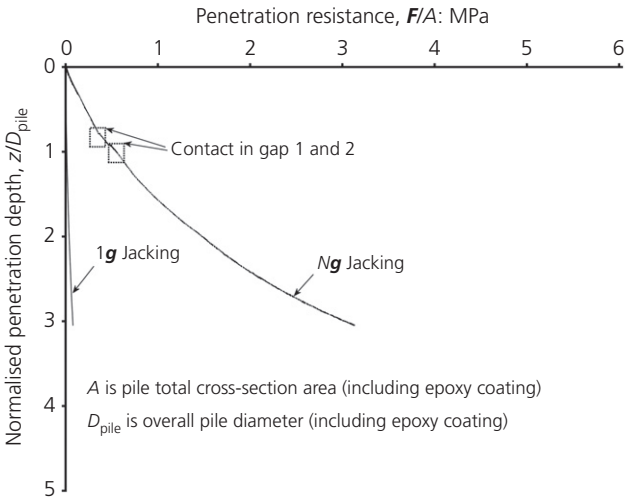

Figure 7. Penetration resistance for jacked installation (1***g*** and ***Ng***)

the total predicted shaft resistance (internal and external) would only be around $F/A \sim 1$ MPa, while the annular tip resistance (assuming full q_c mobilised) would be 1·2 MPa. If plugging occurs, the internal shaft resistance will rise due to arching effects, although it will ultimately be limited by the plugged end-bearing resistance, which may be estimated as $\sim 0{\cdot}6 \times q_c = 4{\cdot}8$ MPa. The measured penetration resistance of 3·1 MPa therefore suggests that full plugging did not occur, but partial plugging must have started.

4.1.2 Impact driving

Figure 8(a) shows the self-weight penetration and cumulative hammer blows recorded during the installation. The pile penetrated to a depth of around $0{\cdot}9D_{pile}$ under its self-weight before being driven. It took 1977 blows to drive the pile to the same embedment length as the jacked installation. The number of blows required per unit penetration increases with the penetration depth, as expected. A driving speed of around 27 blows/m was recorded at shallow depths and around 330 blows/m was reported at the end of the driving, both of which are realistic for prototype conditions.

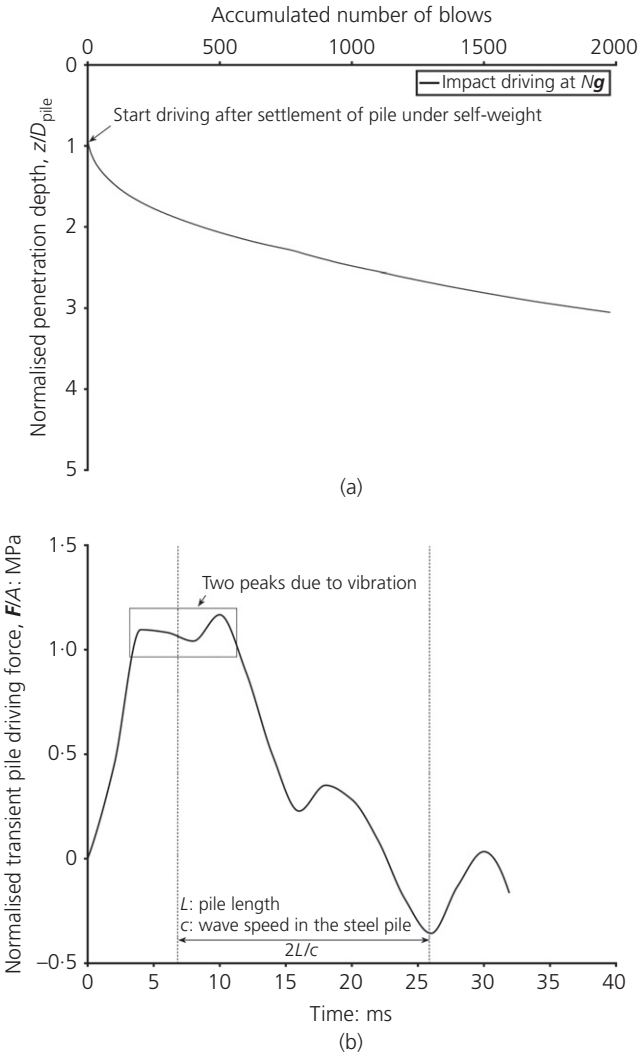

Figure 8. (a) Cumulative hammer blow count plotted against the penetration depth and (b) transient peak impact driving force

Figure 8(b) shows a typical transient impact driving force obtained during trial tests. This is very similar to those reported by Bruno and Randolph (1999) and Heins *et al.* (2018). A peak impact force of around 1·2 MPa was recorded, with two successive peaks observed in each strike. This probably reflects a slight bounce between the pile cap and anvil.

4.2 Pile under monotonic lateral loading

4.2.1 Determination of pile head displacement and rotation

The pile head displacement and rotation (defined at the mudline) are normally used as design criteria in design codes such as DNV (2014). However, displacement measurement directly at the mudline was not feasible due to the difficulty in arranging transducers in a centrifuge test. Instead, the pile displacements were measured at two elevations, 22 mm (0·44D) and 126 mm (2·52D) above the mudline (Figure 4). The pile head displacement and rotation may then be derived using the rigid beam theory or, slightly more accurately, using Euler–Bernoulli or Timoshenko beam theories that account for pile deformation.

Both laser displacement transducers and linear potentiometers have been used in the literature and were trialled in this study. Measuring accuracy of less than 5 μm is required to capture the small displacement response reasonably well, especially during cyclic loading, but a significant displacement range is needed for ultimate capacity. The potentiometers did not perform well due to the excessive transverse forces, and hence friction, when used to measure lateral displacements perpendicular to the high-g field. Contact between the pile and transducer may also result in additional frictional force when the pile penetrates. Therefore, two non-contact laser displacement sensors were used in the tests, allowing displacements and rotations at mudline to be derived.

The displacement profiles allowing for pile deformation can be written as

Euler − Bernoulli beam theory(pure bending)

$$\delta = \frac{H}{6\mathrm{EI}} z^2 (3e - z) \quad (1)$$

2. Timoshenko beam theory (bending + shear)

$$\delta = \frac{H}{6\mathrm{EI}} z^2(3e - z) + \frac{Hz}{\kappa AG}$$

where H is the lateral force applied, z is the distance above mudline, e is the load eccentricity, EI is the pile-bending stiffness, A is the pile cross-sectional area, G is the pile shear modulus and κ is the Timoshenko shear coefficient, with $\kappa = 0{\cdot}90$ for a pipe pile (Faghidian, 2017).

The results of pile head displacement obtained for the different beam theories are indistinguishable, as shown in Figure 9. The lateral displacement is normalised by the pile external diameter (D_{pile}). The lateral force is normalised by $\gamma D_{\mathrm{pile}}^3$, γ is the unit weight of the sand (see Table 2). This indicates that the pile tends to behave as rigid over the relevant length ($z_2 = 2{\cdot}52D$) and the rigid beam theory was therefore used to determine the mudline displacement and rotation throughout.

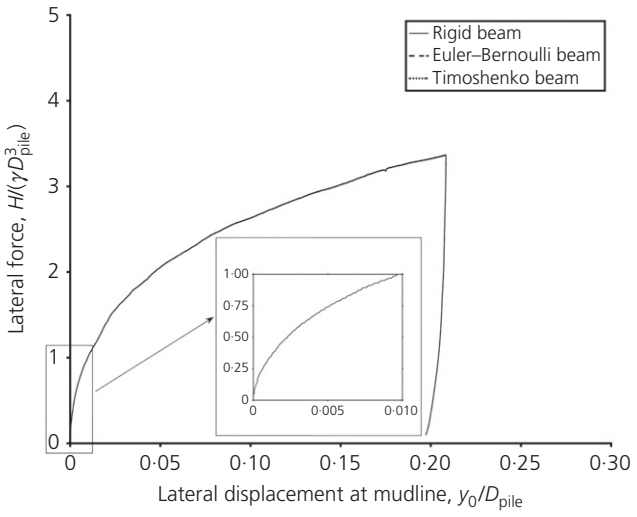

Figure 9. Comparison of the load–displacement curve derived from different beam theories

4.2.2 Effect of pile installation method on the initial stiffness and ultimate capacity

Figure 10 shows the lateral response of monopiles installed by different installation methods. Both qualitative and quantitative comparisons are made. The lateral capacity mobilised at $0{\cdot}1D_{\mathrm{pile}}$ mudline displacement is summarised in Table 3. The initial stiffness (k_{ini}) defined as the tangential stiffness at zero mudline displacement is summarised in Table 4. The secant stiffness (k_{ult}) defined at $0{\cdot}1D_{\mathrm{pile}}$ mudline displacement is also given in Table 4. Only normalised values are given in Tables 3 and 4.

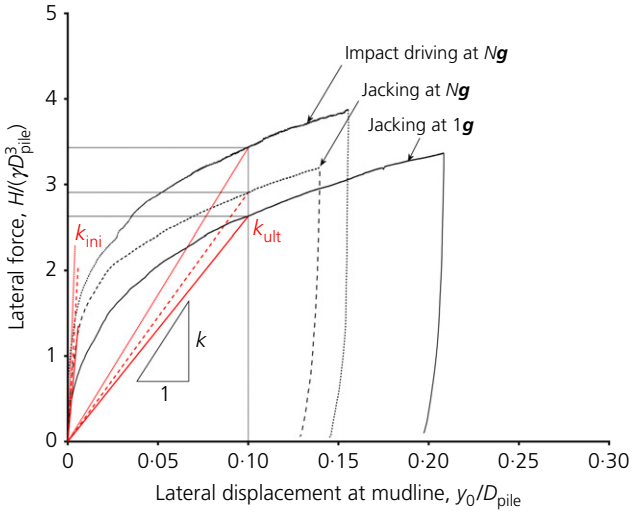

Figure 10. Load–displacement curve

Table 3. Lateral bearing capacity

Test number	Installation method	Capacity mobilised at $y_0/D_{\mathrm{pile}} = 0{\cdot}1$
		Normalised value $H/(\gamma D_{\mathrm{pile}}^3)$: dimensionless
1	Jacking at 100$\boldsymbol{g}$	2·9
2	Jacking at 1$\boldsymbol{g}$	2·6
3	Impact driving at 100$\boldsymbol{g}$	3·4

Table 4. Lateral stiffness

Test number	Installation method	Initial stiffness	Secant stiffness
		Normalised value $H/(y_0\gamma D_{\mathrm{pile}}^2)$: dimensionless	
1	Jacking at 100$\boldsymbol{g}$	354·4	29·1
2	Jacking at 1$\boldsymbol{g}$	233·8	26·3
3	Impact driving at 100$\boldsymbol{g}$	567·3	34·2

The model pile jacked in-flight shows larger initial stiffness than when jacked at 1$\boldsymbol{g}$ due to the retention of high lateral stresses caused by installation. This is in agreement with the findings given by Dyson and Randolph (2001) and Klinkvort (2012). However, the trend of the two curves in Figure 10 suggests that the stress-level effect may ultimately be erased, although this would require large pile head displacement (much greater than $0{\cdot}2D_{\mathrm{pile}}$). In contrast, a pile installed using impact driving shows larger initial stiffness and higher ultimate capacity than the jacked piles. Although the ambient stress

levels were identical in tests where the piles were jacked or driven at Ng, the increased stiffness and ultimate capacity result from changes in the soil state caused by impact driving. According to the numerical investigation by Henke and Grabe (2008), the external horizontal stress in the vicinity of the pile tip is much higher following jacking than following impact driving in a medium dense sand sample with a relative density of 51–55%. Higher vertical stress near the pile tip is also expected following jacking than following impact driving. However, the degree of densification of soil, especially in the upper part of the pile is higher following impact driving than following jacking. In addition, a relatively looser sample with a relative density of $38 \pm 4\%$ was used in this study and thus the degree of densification was judged to be higher. This could be a reasonable explanation for the fact that the impact-driven pile has a higher lateral initial stiffness and ultimate capacity. A stiffer axial response of impact-driven piles than jacked piles was also reported by Heins *et al*. (2018) due to the densification of the surrounding soil caused by impact driving in a sand sample with a similar relative density.

The impact-driven pile has a normalised ultimate capacity of 3·4, which is 15% higher than for the jacked pile (2·9) as shown in Figure 10. The normalised initial stiffness of the impact-driven pile is 567·3, which is 60% higher than for the jacked pile (354·4). The results suggest the foundation stiffness is significantly influenced by the installation method. Offshore wind turbines are dynamically sensitive structures. Further research to characterise the influence of monopile response under cyclic lateral loading is ongoing.

The fatigue and serviceability limit states (FLS and SLS) are key design drivers for offshore monopile foundations, with accurate estimation of the structural natural frequency being particularly important for the FLS design (Arany *et al*., 2015). The system natural frequency of offshore wind turbines is influenced by the foundation stiffness. Therefore changes in soil state due to the installation process should be considered in the design as they will affect the natural frequency of the foundation. To illustrate this point, using the method given by Arany *et al*. (2016), the natural frequency for Burbo Bank Offshore Wind Farm (considered here because the seabed also comprises sandy soil) would increase by 4·2% if the foundation stiffness was increased by 60%; or, it would decrease by 13·8% if the foundation stiffness was reduced by 60%.

5. Conclusions

This paper has detailed the development of a purpose-designed apparatus that allows in-flight pile installation using different installation methods, followed directly by lateral loading without stopping the centrifuge, hence retaining the installation-induced stress state in the soil. All operations can be conducted in-flight and this is one of the few reported centrifuge test series where this is possible. This is deemed particularly important as ramping up and down the centrifuge or any manipulation would change the soil state around the pile. The apparatus makes it possible to replicate field operations including pile installation from the soil surface and lateral loading in a centrifuge.

The results of three lateral loading tests where model monopiles were jacked at $1g$ and Ng and impact driven at Ng into a dry medium dense sand sample were analysed. The following conclusions are drawn from the test results.

- The axial force required to jack the pile to a penetration of 3·1 diameters was 44% higher than would be estimated using the UWA-05 method for driven piles. This suggests higher (average) radial effective stresses around the pile shaft and at the base – that is, with less friction degradation that accompanies the cyclic shearing that occurs during driving.
- The initial stiffness and ultimate capacity of a monopile under lateral loading in a medium dense sand are significantly influenced by the installation process.
  The impact-driven pile shows both higher initial stiffness and larger ultimate capacity than the jacked pile.
  The stress-level effect was also demonstrated through a comparison of piles jacked at $1g$ and Ng, with the latter showing increased stiffness and capacity under lateral loading, as expected.
- The higher stiffness and capacity for the driven pile compared with the jacked pile (both at Ng) may be attributed to the increased density of the sand following driving.
- As a result of the changes in soil state, the installation method will affect the natural frequency of an offshore wind turbine founded on a monopile. In turn, this will influence the FLS design of offshore wind turbines.

Research on the effect of the installation process of the in-service response of monopiles is ongoing. Factors such as pore–fluid response (saturated sand) and the effect of cyclic loading at working load levels are considered. The test results will also be used to validate numerical models, which will be used to extend the research to dense sands and a wider range of pile diameter, wall thickness and embedment length.

Acknowledgements

This work forms part of the activities of the Centre for Offshore Foundation Systems (COFS), which is currently supported as a Centre of Excellence by the Lloyd's Register Foundation and through the Fugro chair in Geotechnics and the Shell EMI chair in Offshore Engineering. Lloyd's Register

Foundation helps to protect life and property by supporting engineering-related education, public engagement and the application of research. This support is gratefully acknowledged. Furthermore, support from the technical staff (John Breen, Manuel Palacios, Adam Stubbs, David Jones, Khin Seint, Mike Turner, Andrew Van Dam and Guido Wager) at the National Geotechnical Centrifuge Facility (NGCF) is gratefully acknowledged.

REFERENCES

Achmus M and Abdel-Rahman K (2005) Finite element modelling of horizontally loaded monopile foundations for offshore wind energy converters in Germany. In *Frontiers in Offshore Geotechnics: Proceedings of the 1st International Symposium on Frontiers in Offshore Geotechnics (ISFOG2005)* (Gourvenec SM and Cassidy MJ (eds)). Taylor and Francis, London, UK, pp. 391–396.

Achmus M, Kuo YS and Abdel-Rahman K (2009) Behavior of monopile foundations under cyclic lateral load. *Computers and Geotechnics* **36(5)**: 725–735, https://doi.org/10.1016/j.compgeo.2008.12.003.

API (American Petroleum Institute) (2011) *Recommended Practice 2GEO – Geotechnical and Foundation Design Considerations*, 1st edn. API, Washington, DC, USA.

Arany L, Bhattacharya S, Macdonald JHG and Hogan SJ (2015) A critical review of serviceability limit state requirements for monopile foundations of offshore wind turbines. *Proceedings of the Offshore Technology Conference, Houston, TX, USA*, paper OTC-25874-MS.

Arany L, Bhattacharya S, Macdonald JHG and Hogan SJ (2016) Closed form solution of eigen frequency of monopile supported offshore wind turbines in deeper waters incorporating stiffness of substructure and SSI. *Soil Dynamics and Earthquake Engineering* **83**, 18–32, https://doi.org/10.1016/j.soildyn.2015.12.011.

Bienen B, Dührkop J, Grabe J, Randolph MF and White DJ (2012) Response of piles with wings to monotonic and cyclic lateral loading in sand. *Journal of Geotechnical and Geoenvironmental Engineering* **138(3)**: 364–375, https://doi.org/10.1061/(asce)gt.1943-5606.0000592.

Bruno D and Randolph MF (1999) Dynamic and static load testing of model piles driven into dense sand. *Journal of Geotechnical and Geoenvironmental Engineering* **125(11)**: 988–998, https://doi.org/10.1061/(asce)1090-0241(1999)125:11(988).

Byrne BW, McAdam R, Burd HJ *et al.* (2015) New design methods for large diameter piles under lateral loading for offshore wind applications. In *Frontiers in Offshore Geotechnics III: Proceedings of the 3rd International Symposium on Frontiers in Offshore Geotechnics (ISFOG2015)* (Meyer V (ed.)). Taylor and Francis, London, UK, pp. 10–12.

Byrne BW, McAdam RA, Burd H *et al.* (2017) PISA: new design methods for offshore wind turbine monopiles. In *Offshore Site Investigation and Geotechnics (OSIG) – Smarter Solutions for Future Offshore Developments: Proceedings of the 8th International Conference.* Society for Underwater Technology, London, UK, vol. 1, pp. 142–161.

Chow SH, O'Loughlin CD, Gaudin C and Lieng JT (2018) Drained monotonic and cyclic capacity of a dynamically installed plate anchor in sand. *Ocean Engineering* **148**: 588–601.

De Nicola A (1996) *The Performance of Pipe Piles in Sand.* Doctoral dissertation, University of Western Australia, Perth, Australia.

De Nicola A and Randolph MF (1994) Development of a miniature pile driving actuator. In *Centrifuge 94: Proceedings of the International Conference Centrifuge 94* (Lee FH, Leung CF and Tan TS (eds)). Balkema, Rotterdam, the Netherlands, pp. 473–478.

De Nicola A and Randolph MF (1997) The plugging behaviour of driven and jacked piles in sand. *Géotechnique* **47(4)**: 841–856, https://doi.org/10.1680/geot.1997.47.4.841.

DIN (2014) EN 10088-3: Stainless Steels – Part 3: Technical Delivery Conditions for Semi-Finished Products, Bars, Rods, Wire, Sections and Bright Products of Corrosion Resisting Steels for General Purposes. DIN, Berlin, Germany.

DNV (Det Norske Veritas) (2014) Offshore Standard DNV-OS-J101 – Design of Offshore Wind Turbine Structures. DNV, Hoevik, Norway.

Dyson GJ and Randolph MF (2001) Monotonic lateral loading of piles in calcareous sand. *Journal of Geotechnical and Geoenvironmental Engineering* **127(4)**: 346–352, https://doi.org/10.1061/(asce)1090-0241(2001)127:4(346).

EWEA (European Wind Energy Association) (2017) *Offshore Wind in Europe – Key Trends and Statistics 2017*. European Wind Energy Association, Brussels, Belgium.

Faghidian SA (2017) Unified formulations of the shear coefficients in Timoshenko beam theory. *Journal of Engineering Mechanics* **143(9)**: 06017013, https://doi.org/10.1061/(asce)em.1943-7889.0001297.

Gaudicheau P, Thorel L, Néel A *et al.* (2013) Improvement of the IFSTTAR robot control system. In *ICPMG2014 – Physical Modelling in Geotechnics* (Gaudin C and White D (eds)). CRC Press, Leiden, the Netherlands, vol. 1, pp. 221–226.

Haffar IEL, Blanc M and Thorel L (2017) Impact of pile installation method on the axial capacity in sand. *Géotechnique Letters* **7(3)**: 260–265, https://doi.org/10.1680/jgele.17.00036.

Heins E, Bienen B, Randolph MF and Grabe J (2018) Effect of installation method on static and dynamic load test response for piles in sand. *International Journal of Physical Modelling in Geotechnics*, https://doi.org/10.1680/jphmg.18.00028.

Henke S and Bienen B (2013) Investigation of the influence of the installation method on the soil plugging behaviour of a tubular pile. In *ICPMG2014 – Physical Modelling in Geotechnics* (Gaudin C and White D (eds)). CRC Press, Leiden, the Netherlands, vol. 2, pp. 681–687.

Henke S and Grabe J (2008) Numerical investigation of soil plugging inside open-ended piles with respect to the installation method. *Acta Geotechnica* **3(3)**: 215–223, https://doi.org/10.1007/s11440-008-0079-7.

Klinkvort RT (2012) *Centrifuge Modelling of Drained Lateral Pile-Soil Response.* Doctoral dissertation, Technical University of Denmark, Lyngby, Denmark.

Klinkvort R and Hededal O (2010) Centrifuge modelling of offshore monopile foundation. In *Frontiers in offshore Geotechnics II: Proceedings of the 2nd International Symposium Frontiers in Offshore Geotechnics (ISFOG2010)* (Gourvenec SM and White D (eds)). Taylor and Francis, London, UK, pp. 581–586.

Labenski J, Moormann C, Aschrafi J and Bienen B (2016) Simulation of the plug inside open steel pipe piles with regards to different installation methods. In *Proceedings of 13th Baltic Sea Geotechnical Conference* (Kuliešius V, Bondars K and Ilves P (eds)). Vilnius Gediminas Technical University, Vilnius, Lithuania, pp. 223–230.

Leblanc C, Houlsby GT and Byrne BW (2010) Response of stiff piles in sand to long-term cyclic lateral loading. *Géotechnique* **60(2)**: 79–90, https://doi.org/10.1680/geot.7.00196.

Lehane BM, Schneider JA and Xu X (2005) *A Review of Design Methods for Offshore Driven Piles in Siliceous Sand*. The University of Western Australia, Perth, Australia, UWA Report No. GEO 05358.

Mahutka KP, König F and Grabe J (2006) Numerical modelling of pile jacking, driving and vibratory driving. In *Proceedings of International Conference on Numerical Simulation of Construction Processes in Geotechnical Engineering for Urban Environment (NSC06), Bochum* (Triantafyllidis T (ed.)). Balkema, Rotterdam, the Netherlands, pp. 235–246.

Matlock H (1970) Correlation for design of laterally loaded piles in soft clay. *Proceedings of the Offshore Technology Conference, Houston, TX, USA*, paper OTC-1204-MS.

Randolph MF and Gaudin C (2017) Genesis of the National Geotechnical Centrifuge Facility – a 30 year perspective. *Australian Geomechanics* **52(2)**: 1–17.

Reese LC, Cox WR and Koop FD (1974) Analysis of laterally loaded piles in sand. *Proceedings of the Offshore Technology Conference, Houston, TX, USA*, paper OTC-2080-MS.

Schneider J and Lehane B (2006) Effects of width for square centrifuge displacement piles in sand. In *Physical Modelling in Geotechnics: Proceedings of the 6th International Conference on Physical Modelling in Geotechnics (ICPMG2006)* (Ng CWW, Wang YH and Zhang LM (eds)). Taylor and Francis, London, UK, vol. 2, pp. 867–873.

Tran MN (2005) *Installation of Suction Caissons in Dense Sand and the Influence of Silt and Cemented Layers*. Doctoral dissertation, The University of Sydney, Sydney, Australia.

Verdure L, Garnier J and Levacher D (2003) Lateral cyclic loading of single piles in sand. *International Journal of Physical Modelling in Geotechnics* **3(3)**: 17–28, https://doi.org/10.1680/ijpmg.2003.030303.

Zdravković L, Taborda DMG, Potts DM *et al.* (2015) Numerical modelling of large diameter piles under lateral loading for offshore wind applications. In *Frontiers in Offshore Geotechnics III: Proceedings of the 3rd International Symposium on Frontiers in Offshore Geotechnics (ISFOG2015)* (Meyer V (ed.)). Taylor and Francis, London, UK, pp. 759–764.